A Few Good Responses: Which Mechanical Effects of IOP on the ONH to Study?

Ian A. Sigal[1,2,3] *and Jonathan L. Grimm*[1]

Purpose. The biomechanical effects of IOP on the optic nerve head (ONH) are believed to play a role in glaucomatous neuropathy. There is, however, no consensus on which effects of IOP should be prioritized for investigation. Our goal was to identify a small set of variables capturing the majority of the effects of acute IOP on the ONH.

Methods. We produced 4646 finite element models of the human ONH representing a wide range of tissue anatomies and mechanical properties. The effects of IOP were quantified through a set of 25 responses including stress, strain, and geometric deformation of the lamina cribrosa (LC) and peripapillary sclera. The correlations between the responses were analyzed and principal component analysis (PCA) was used to identify uncorrelated variables capturing the largest possible variance in the responses.

Results. The responses formed groups with strong correlations. The top five principal components (PCs) accounted for 72.8%, 13.0%, 7.1%, 3.1%, and 2.0% of the variance, respectively.

Conclusions. Few PCs capture the majority of the mechanical effects of acute changes in IOP on the ONH, which previously required 25 measures. The PCs represented four key effects of IOP: lateral deformation associated with canal expansion (PC1), anterior-posterior deformation of the LC and the forces through it determined by either the mechanical properties of the LC (PC2) or of the neural tissue (PC4), rotation of the peripapillary sclera (PC5), and forces through the peripapillary sclera (PC3). A small set of uncorrelated variables will simplify describing and understanding the effects of IOP on the ONH. (*Invest Ophthalmol Vis Sci.* 2012;53:4270–4278) DOI: 10.1167/iovs.11-8739

Glaucoma is one of the leading causes of blindness worldwide.[1] The causes of retinal ganglion cell (RGC) degeneration in glaucoma are not understood, but elevated IOP has been identified as a primary risk factor for the development and progression of glaucomatous optic neuropathy. A biomechanical theory of glaucoma proposes that mechanical effects on the tissues of the optic nerve head (ONH) are, at least in part, responsible for the damaging effects of IOP.[2,3] There is consensus in the literature regarding the importance of understanding the biomechanical effects of IOP on the ONH. There is no consensus, however, on which effects of IOP on the ONH should be prioritized for investigation. Authors have considered many aspects of the response of the ONH depending on their hypotheses of how IOP affects RGCs and also the technology available.

Analyzing few responses risks missing critical effects of IOP, and to avoid this problem researchers often study many responses. Some recent studies, for example, have analyzed 13,[4] 17,[5] or 29[6] responses to IOP. Considering regional effects, the number of responses analyzed has reached 79.[7] There are drawbacks, however, in simultaneously studying many responses. First, there is the challenge of keeping track and making sense of many variables. Many of these responses are independently complex and, thus, evaluating several of them simultaneously becomes problematic.[8] Second, many of the responses are correlated, further complicating the analysis and interpretation.[9]

We hypothesized that the ONH responds to variations in IOP as a system, and, therefore, that the various responses are related. We propose that it is possible to find a small set of responses that are uncorrelated and comprehensively represent the biomechanical effects of IOP on the ONH. In other words, we propose that with only a few carefully chosen variables it is possible to describe the mechanical response of an ONH to IOP.

The objective of this work was, therefore, to use dimensionality reduction techniques, principal component analysis (PCA) in particular, to identify a small set of uncorrelated variables that describe the variance in ONH response to acute changes in IOP that traditionally has been measured with many correlated responses.

Methods

The general strategy was to produce many models of the ONH with varying tissue geometry and material properties. Finite element (FE) modeling was used to predict the effects on each of the models of an acute increase in IOP, and a set of 25 responses was used to quantify these effects. We analyzed the correlations between the responses, and used PCA to identify noncorrelated variables that represent the largest possible variance in the responses. Below, we describe each of the steps in detail. The rationales for the choices made, and of their consequences are addressed in the Discussion section.

Modeling

We generated 4646 models of ONHs with carefully controlled variations in parameters describing tissue geometry and material properties (Table 1). These parameters were the globe radius, scleral thickness and modulus (stiffness), lamina cribrosa radius, anterior-posterior position and modulus, neural tissue modulus, and prelaminar

From the Departments of [1]Ophthalmology and [2]Bioengineering, University of Pittsburgh, Pittsburgh, Pennsylvania; and the [3]McGowan Institute for Regenerative Science, University of Pittsburgh School of Medicine, Pittsburgh, Pennsylvania.

Supported by grants from the National Institutes of Health (P30EY008098), the Eye and Ear Foundation, and unrestricted grants from Research to Prevent Blindness.

Submitted for publication October 4, 2011; revised March 19, 2012; accepted April 26, 2012.

Disclosure: **I.A. Sigal**, None; **J.L. Grimm**, None

Corresponding author: Ian A. Sigal, Laboratory of Ocular Biomechanics, Department of Ophthalmology, University of Pittsburgh, 203 Lothrop Street, Room 930, Pittsburgh, PA 15213; sigalia@upmc.edu.

Table 1. Model Parameters and the Ranges over Which They Were Varied

Parameter	Short Name	Minimum	Maximum
Globe radius	Eye radius	9.6 mm	14.4 mm
Scleral thickness	Sc thick	0.64 mm	0.96 mm
Lamina cribrosa radius	LC radius	0.76 mm	1.14 mm
Prelaminar tissue compressibility (Poisson's ratio)	Poisson	0.40	0.49
Neural tissue modulus	NT modulus	0.01 MPa	0.09 MPa
Laminar modulus	LC modulus	0.1 MPa	0.9 MPa
Scleral modulus	Sc modulus	1.0 MPa	9.0 MPa
Laminar position	LC depth	0.0 mm	0.2 mm

tissue compressibility. The biomechanical effects of an increase of 10-mmHg in IOP were predicted for each case using commercial FE software (Ansys v11; Ansys Inc., Canonsburg, PA). The eight parameters varied in this study were selected based on a preliminary multivariate sensitivity analysis on 21 parameters.[8,10] In the preliminary study, it was found that the eight parameters, and their interactions, accounted for between 97.7% and 99.9% of the variance in the responses. The 13 parameters not varied here were set at their baseline levels used in our previous work.[6,8] The parameter combinations modeled were selected based on a response surface analysis methodology.[10,11]

The base model was defined to represent a low IOP (5 mm Hg) and the IOP increases modest (up to 10 mm Hg). The apex of the anterior pole was constrained in all directions to prevent displacement or rotation. The effects of IOP were modeled as a distributed load acting on the surfaces exposed to the interior of the eye. All tissues were assumed linearly elastic, isotropic, and homogeneous.[6,8,10,12–15] Tissue stiffnesses were defined by Young's moduli

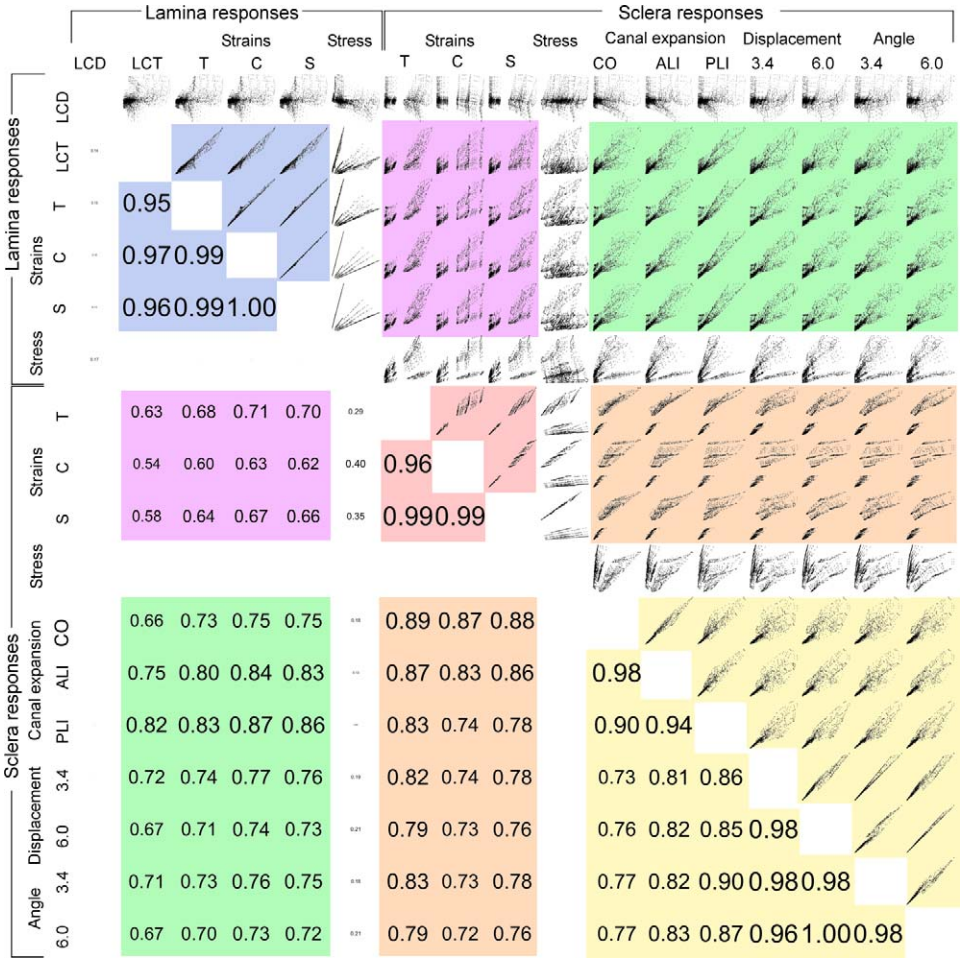

Figure 1. Matrix of scatterplots (*top right*) and correlation strengths (adjusted-R^2's, *bottom left*) between the responses. Each point on a scatterplot represents a model. The responses formed groups with strong correlations. These groups are highlighted with colors. To reduce the size and complexity of an already large plot, only some responses are included. Peak and median measures were highly correlated (all correlations above 0.99), and, therefore, only the medians are shown. Since the mean stresses were poorly correlated with other responses, the stresses appear as blank rows and columns. The font size of the correlations is proportional to the magnitude of the correlation strength to emphasize the strong correlations and de-emphasize the weak ones. LCD, lamina cribrosa displacement; LCT, lamina cribrosa thinning; T, tensile (strain); C, compressive (strain); S, shear (strain); CO, Canal opening; ALI, Anterior lamina insertion; PLI, Posterior lamina insertion. See the Methods section for details of how the responses were computed.

and compressibilities by Poisson's ratios. All tissues, other than the prelaminar neural tissue were assumed incompressible. As in our previous sensitivity analyses,[6,8,12,14] we use stiff and compliant to describe high and low Young's moduli, respectively. Thus, stiffness is equivalent to the tissue's mechanical property and is independent of the geometry. The parameters and their ranges have been discussed in detail elsewhere.[6,8,12–14] Further details of the development, processing, simulation, and analysis of the FE models are described elsewhere.[6,8,12]

Responses

Twenty five measures, or responses, were used to characterize the effects of IOP on the ONH, divided into the following groups:

Nine geometrical measures:

- The anterior-posterior lamina cribrosa displacement (LCD), measured as the change in the anterior-posterior position of the anterior lamina cribrosa surface with respect to the anterior lamina insertion into the sclera[9];
- The thinning of the lamina cribrosa (LCT) measured at the center of the canal and cup[16];
- The scleral canal expansion at the scleral canal opening (SCE_CO), at the anterior lamina insertion (SCE_ALI), and at the posterior lamina insertion (SCE_PLI)[16,17]; and
- The response of the peripapillary sclera measured at two points on the anterior surface 1.7 and 3.0 mm from the axis of symmetry. These points mimic rings 3.4 and 6.0 mm in diameter, which have been proposed to measure peripapillary sclera bowing in response to IOP.[3,4,18] At each of these points we measured the anterior-posterior displacements (Sc_D_3.4 and Sc_D_6.0) and the rotations (Sc_R_3.4 and Sc_R_6.0); that is, the change in angle with respect to the axis of symmetry.

Sixteen measures of tissue strain and stress:

- The tensile, compressive and shear strains representing the maximum local tissue stretch, and compression and shear, which are computed from the maximum and minimum principal strains[19];
- The stresses as were quantified by the Von Mises Equivalent stress. The Von Mises stress gives an indication of the forces acting through the tissue, while discounting the effects of hydrostatic pressure. It is commonly used in studies of ONH biomechanics in lieu of the tensor of stress, and in engineering to predict the tendency of materials to fail.[6,12–14,17,20,21]

  We captured the variation in strains and stress over the tissues by computing the 50th and 95th percentiles of their distributions, representing the median and peak. Using these measures, rather than the mean and maximum reduces the influence of numerical artifacts, or of regions too small to have physiologic significance.[13] The strains and stress in the sclera were computed in regions within 5° of the axis of symmetry (the peripapillary scleral flange).

  Peak and median values of three strains and a stress for each of the LC and the sclera amount to 16 responses for each model.

Analysis

To determine the extent to which all the responses were associated we computed the correlation matrix (*R* v2.12.0).[22] Associations between variables are often studied using the covariance matrix. Covariances, however, are sensitive to the units, or scale, in which a response is measured making a comparison between multiple variables in different units difficult. We did not have this problem since all variables were scaled prior to analysis to have the same variance.[23,24]

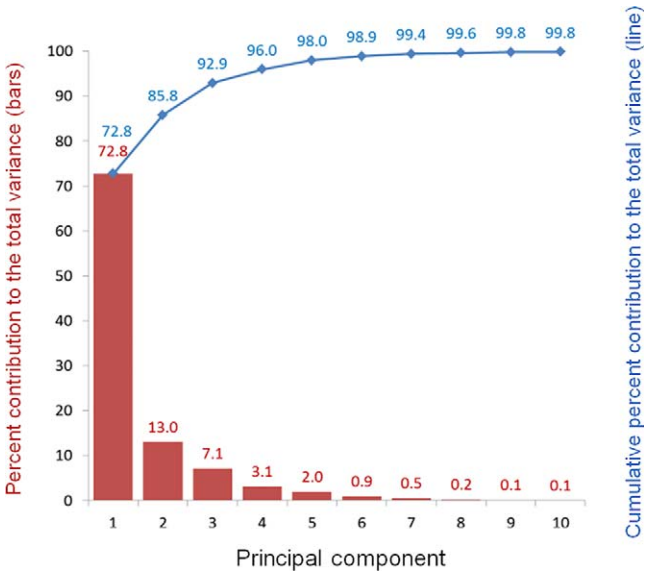

Figure 2. Graphical representation of the absolute (*bars*) and cumulative (*lines*) contributions of the top 10 PCs to the total variance in 25 responses. PC1 accounted for almost three quarters of the variance. The top four PCs accounted for 96% of the variance, and seven PCs are needed to account for over 99% of the variance. This demonstrates that there was substantial redundancy in the use of 25 variables to describe the ONH. See Table 1 for a list of the responses included in each analysis. The top three PCs are special because they each account for over 4% in response variances. If all the responses had been independent, for example, perfectly uncorrelated, then each PC would correlate with a single response and account for 1/25 (4%) of the variance.

For dimensionality reduction we used PCA on the responses.[25,26] PCA involves computing the eigenvectors and eigenvalues of the correlation matrix of the responses. The eigenvectors describe independent patterns in the variation of the responses. In PCA, these new variables are called the principal components (PCs), and are ordered according to the amount of variance they account for. In this sense, PC1 is the variable with the largest variance, PC2 has the second largest variance and is orthogonal to PC1 (i.e., PC1 and PC2 are uncorrelated), PC3 has the third largest variance and is orthogonal to PC1 and PC2 (i.e., PC3 is uncorrelated with both PC1 and PC2), and so on and so forth.

Results

The responses formed groups with strong correlations (Fig. 1). The strains were highly correlated with each other within the same tissue, but not so strongly between tissues. Lamina strains were also highly correlated with LCT, and less strongly with canal expansions, and the sclera displacements and rotations. The stresses were also highly correlated with each other within a tissue, but not between tissues or with other responses. Canal expansions were highly correlated with each other, with the rotations of the sclera, and with the strains. LCD was not well correlated with anything.

The high correlations between the responses were evidence of substantial redundancy in the set of 25 responses. This was confirmed with the PCA (Fig. 2). A small number of PCs was sufficient to account for the majority of the variance in the responses. Four PCs accounted for 96% of the variance in 25 responses. If all 25 responses had been independent, each of them would contribute 4% to the total variance, and each PC would describe 4% of the variance.

Biplots of the top four PCs help understand the relationship between PCs, responses, and parameters (Figs. 3, 4). PC1

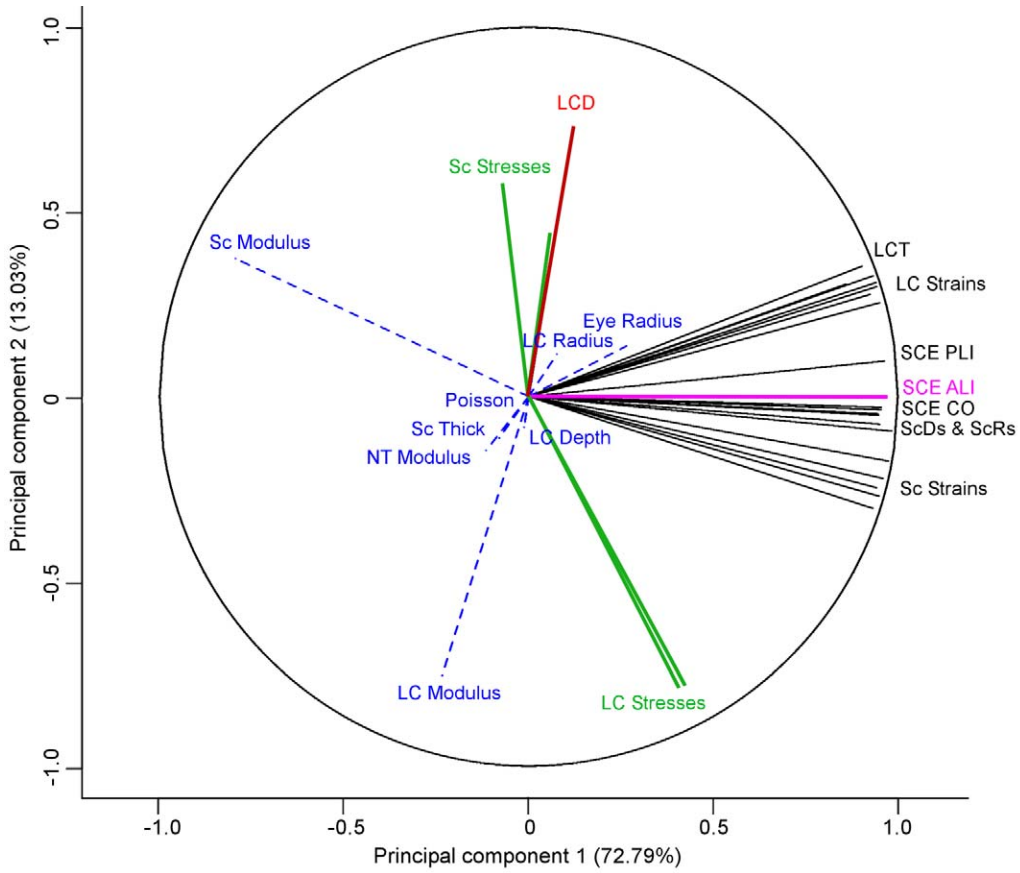

Figure 3. Biplot of the top two principal components, PC1 and PC2. A biplot shows two-dimensional projections of the responses (*continuous lines*) and parameters (*dashed lines*). The angle between lines represents the strength of the correlation between variables. Strongly correlated variables are parallel (0°) or anti-parallel (180°), and independent variables are orthogonal (90°). All lines have a length of 1 in a 25-dimensional space. Line length in a biplot is the variance accounted for by the two PCs. PC1 accounted for the majority of the variance and was highly correlated with responses of the sclera. PC2 accounted for less variance and was highly correlated with LCD. Lamina modulus is antiparallel to LCD, showing that increased lamina modulus was associated with decreased LCD. LCD increased with lamina radius. The parameters were not included when computing the PCs and are shown only as covariates to illustrate their relationship with the responses and the PCs.

accounted for 72.8% of the variance and was highly correlated with many responses including lamina and sclera strains, canal expansions, and sclera displacement and rotation of the peripapillary sclera. Of the parameters, PC1 was most strongly associated with sclera modulus. PC2 explained 13% of the variance, and was highly correlated with LCD and with the stresses, especially those in the lamina. Of the parameters, PC2 was most strongly associated with the lamina and sclera moduli. PC3 accounted for 7.1% of the variance and was most strongly correlated with the stresses in the sclera. Of the parameters PC3, was most strongly associated with the globe size and the scleral shell thickness. PC4 accounted for 3.06% of the variance and was most strongly correlated with LCD and lamina stresses, although these correlations were weak. Of the parameters, PC4 was associated with the lamina depth, and the neural tissue moduli. PC1 was not well correlated with the stresses or LCD. The stresses in the lamina and LCD were correlated with PC2 and PC4. The stresses in the sclera were correlated with PC3 and PC2. Numerical measures of the strength of the correlations between PCs, responses, and parameters for the top six PCs are provided in Figure 5.

Discussion

Our goal was to identify a small set of responses with which it will be convenient to describe the mechanical effects of an acute increase in IOP on the ONH. We have shown not only that this is possible, but also that responses obtained, the PCs, have several useful properties. The PCs are uncorrelated. Additionally, since PCs are ordered according to the variance they capture, it is possible to select the number of PCs to use for capturing the desired variance. The first four PCs accounted together for 96% of the variance, and separately for 72.8%, 13.0%, 7.1%, and 3.1% for PC1, PC2, PC3, and PC4, respectively. This means that with only a few PCs it is possible to describe the effects of IOP on the ONH that previously would have required 25 responses, which is a reduction of 84% in the number of variables.

An oft-cited disadvantage of using PCs derived from dimensionality reduction techniques, such as PCA, is that they may not correspond with standard responses, and therefore PCs may be difficult to interpret.[26] In this study, however, it was found that the top PC's were similar to standard responses and easy to interpret. We suggest the following interpretations based on the biplots (Figs. 3, 4), the correlations between PCs, parameters, and responses (Fig. 5), and their previous results of ONH biomechanics[6,8,9,12–14,19,27]: PC1 was associated with many responses, but most closely it corresponded with the expansion of the scleral canal and the peak strain within the sclera. PC1 was correlated most strongly with the sclera stiffness (inversely). This is consistent with the large influence of scleral properties on many effects of IOP on the ONH,

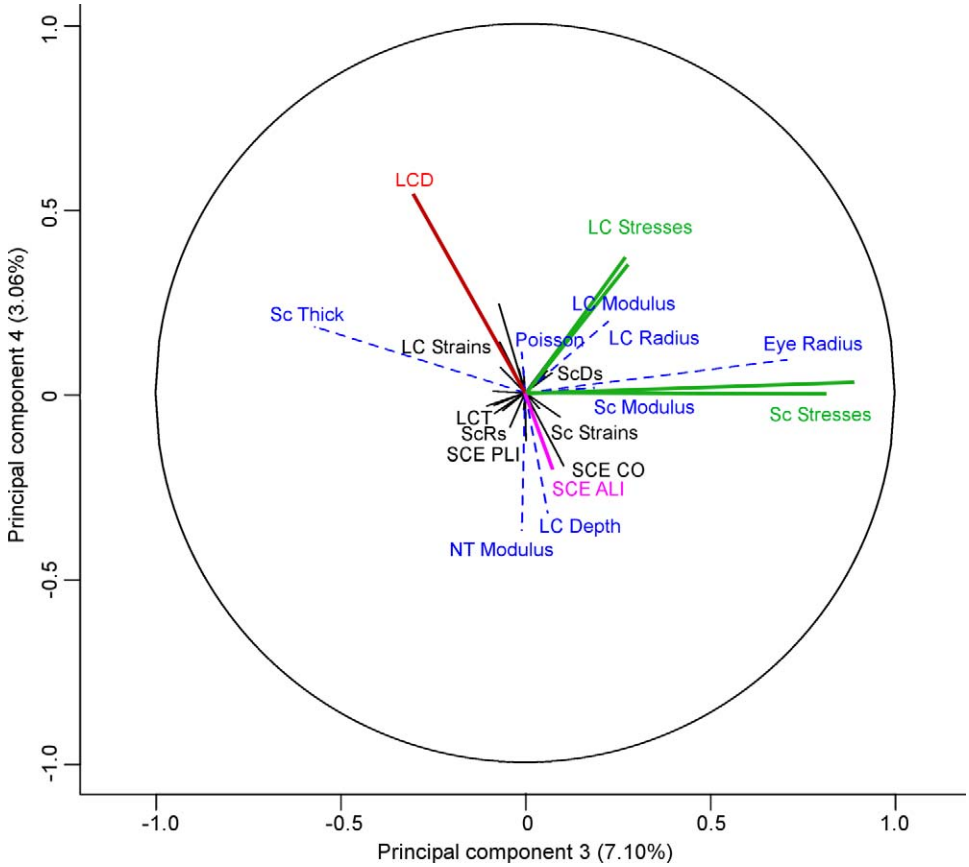

Figure 4. Biplot of PC3 and PC4, with the same formatting as in Figure 3. PC3 was highly correlated with the stresses in the sclera. The stresses in the sclera are close to parallel with the globe radius and scleral modulus, showing that increased globe radius or scleral modulus lead to increased stresses in the sclera. Conversely, the stresses in the sclera are close to antiparallel to the scleral thickness, showing that increased scleral thickness leads to decreased stresses in the sclera.

which we[8,9,12–14,17,21,28] and others[29–32] have reported before. PC2 correlated with the lamina stresses and LCD, and was most strongly influenced by the material properties of the lamina. A stiffer lamina would transmit forces through the canal. Hence, PC2 was associated with the sclera stresses, such that increased lamina stiffness was associated with increased lamina stresses, and decreased sclera stresses and LCD. PC3 was also associated with the sclera stresses, which depend most strongly on the globe size (directly) and the thickness of the shell (inversely). PC4 correlated with LCD and the lamina stresses, explaining the variance in these two responses due to the stiffness of the neural tissues and the lamina position. PC5 represented the displacement and rotation in the peripapillary sclera that were not accounted for by PC1. These responses depended mostly on the size of the globe and the thickness of the shell (e.g., the peripapillary sclera displaces more in large eyes and bends more in thin eyes). Other PCs account for less than 1% of the variance.

The PCs can also be interpreted to mean that there were essentially four types of response to increases in IOP: (1) A lateral deformation associated with the expansion of the canal (PC1), its magnitude determined mainly by the stiffness of the sclera, (2) an anterior-posterior deformation of the lamina associated with forces through it, whose magnitudes are determined by either the stiffness of the lamina (PC2), or by the stiffness of the neural tissue and the position of the lamina (PC4), (3) a rotation of the peripapillary sclera determined by the globe size and the scleral thickness (PC5), and (4) forces induced through the peripapillary sclera (PC3).

These results suggest that our previous studies, focusing on only two effects of IOP on the ONH, namely SCE and LCD, are likely more representative than may appear at first sight.[9,15] Similarly, measuring LCD solely, or responses highly correlated with it, may capture only a small fraction of the effects of IOP. Most recent studies based on three-dimensional histomorphometry or spectral domain optical coherence tomography (SD-OCT) study this type of measure.[4,5,7,33–37] Some studies also included measures of IOP-induced changes in prelaminar tissue volumes, some of which may be more closely associated with canal expansion than with LCD.

Both LCD and SCE present challenges for measuring. A portion of the lamina is behind vasculature, or the tips of the sclera, and is, thus, difficult to detect (more so in the human than in the pig or monkey).[34,38–40] Recent developments, such as Enhanced Depth Imaging,[41] compensation techniques,[39] polarization,[42] or adaptive optics[43,44] show promise in improving imaging of the anterior LC. It is still unclear if these will be sufficient to consistently detect the posterior lamina. The canal opening, although easier to detect, is more difficult to measure accurately because the lateral resolution of OCT is much lower than the axial one. Further complicating these measurements is the fact that the magnitude of the canal expansions is smaller (median 3.6 μm; range from 1 to 33 μm) than the magnitude of LCD (median 8.3 μm; range from −57 to 89 μm). Nevertheless, IOP-induced displacements of both the LC and the scleral canal have been observed in experiments.[5,31,45–48]

Parameters	PC1	PC2	PC3	PC4	PC5	PC6	Total
Globe radius	7	2	50	1	8	4	72
Laminar position	0	1	0	11	1	15	28
Laminar modulus	6	57	5	4	1	0	73
Lamina cribrosa radius	1	1	2	3	2	6	15
Neural tissue modulus	1	2	0	14	1	7	26
Prelaminar tissue compressibility	0	0	0	1	0	3	4
Scleral modulus	63	14	4	0	0	1	82
Scleral thickness	1	1	32	3	19	11	67
Responses							
Sclera rotation ScR_3.4	91	0	0	0	8	0	100
Sclera rotation ScR_6.0	90	0	1	0	8	1	99
Sclera displacement ScD_3.4	91	0	0	0	7	0	99
Sclera displacement ScD_6.0	90	0	0	0	8	1	100
Lamina median tensile strain	87	11	1	0	1	0	100
Lamina median compressive strain	89	9	1	0	0	0	99
Lamina median shear strain	88	10	1	0	0	0	99
Lamina median von Mises stress	18	61	8	12	0	0	98
Lamina peak tensile strain	74	9	0	6	5	4	99
Lamina peak compressive strain	90	6	0	0	1	1	100
Lamina peak shear strain	85	8	0	2	2	2	100
Lamina peak von Mises stress	16	62	7	13	0	0	99
Lamina cribrosa displacement LCD	1	53	9	29	0	7	99
Lamina cribrosa thinning LCT	82	12	1	0	0	0	96
Sclera median tensile strain	92	5	0	0	0	1	99
Sclera median compressive strain	87	9	0	0	2	1	99
Sclera median shear strain	90	7	0	0	1	1	100
Sclera median von Mises stress	0	19	79	0	0	1	99
Sclera peak tensile strain	97	1	0	1	0	0	99
Sclera peak compressive strain	89	6	1	0	2	0	98
Sclera peak shear strain	95	3	0	1	0	0	100
Sclera peak von Mises stress	1	33	66	0	0	0	99
Canal expansion at canal opening	90	1	1	4	1	0	97
Canal expansion at anterior lamina insertion	94	0	1	4	0	0	99
Canal expansion at posterior lamina insertion	93	1	0	2	2	1	98
Fraction of variance for the PC	74	13	7	3	2	1	

Figure 5. Strength of the correlations between PCs, parameters and responses for the top six PCs. Cells are colored in red according to the magnitude of the number in the cell (*red* = 100% and *white* = 0%) to ease noticing the patterns. The variance in many variables was accounted for by PC1, which was associated most strongly with the scleral modulus, consistent with this parameter having a very strong influence on most responses, but not including the stresses or LCD. PC2 was associated with lamina modulus accounting for most of the variance in lamina stress and LCD. PC3 was associated with globe size and sclera thickness, and accounted for the variance in stress in the sclera. Interestingly, the stresses in the sclera were associated with the size and thickness of the globe, and not with its stiffness. PC4 was weakly associated with neural tissue properties and lamina cribrosa position, and accounted for most of the variance in lamina stress and LCD that was not explained by PCs 2 and 3. PC5 accounted for a small amount of variance, mostly from the displacement and rotation of the peripapillary sclera. The total response variances (*rightmost column*) do not all add to 100% because of rounding and variances in higher PCs. The PCs are obtained as linear combinations of the responses. The numbers in this table indicate the contribution of each response to the PC (the square root of these numbers is called the "loading").

The results also show that when analyzing the LC as a homogenized continuum, not much knowledge would be gained by analyzing multiple highly correlated responses, such as the median and peak values of a strain mode. This explains that in the comprehensive sensitivity analyses we obtained essentially the same results for the median and peak values of a mode of strain.[6,8,14] It is important to point out that the PCs represent the variance of the responses considered in the PCA. It is unknown if other responses will be represented or not. This study was repeated with 56 responses (results not shown) adding measures of stress and strain within the pre- and postlaminar neural tissues and the pia mater, as well as some measures of deformation of the cup. It was found that the PCs were consistent in both studies, although two more PCs were required to reach 96% of the variance in 56 measures. There are many other potential responses that were not considered in this study, such as the measures of volume change mentioned above. Particularly important will be to determine whether the results presented here extend to larger variations in IOP, and how regional predictions may depend on local characteristics of the lamina cribrosa, which could affect their covariations. The techniques demonstrated in this work can be applied to other sets of responses, including those from experiments. Depending on the nature of the relationships between the responses it may be necessary to use other dimensionality reduction techniques such as independent component analysis.[49] Although PCA is based on linear regressions, it can be used to study nonlinear relationships by transforming the variables.[26] We repeated this study with various sets of transformations from the Box-Cox family.[11,23] Although there were slight variations, the results were consistent. For clarity, we present the results obtained using untransformed variables. Similarly, the response variances observed depended on the parameters varied and their ranges. The parameters were selected using a multivariate sensitivity analysis of only some of the responses in this work. It is possible that the responses could be sensitive to parameters that were not varied. The parameters were varied independently, which allows for the more general analysis. It is possible that these parameters covary, which would result in further covariations in the responses they influence, affecting the number and structure of the PCs needed to describe them. A reader should also recall that it is not the same that the PCs can account for the vast majority of the variance in the responses as representing explicitly the relationship between responses. However, the successful dimensionality reduction suggests that this may be possible as well.

It is also important to interpret the results in the context of the limitations in the models. We assumed a generic simplified axisymmetric geometry, which does not consider some of the complexities and details of specific ONHs, such as regional material properties. The models, for example, did not incorporate variations in connective tissue densities and composition between the anterior and posterior LC,[21,50,51] or in the fiber orientations between the inner and outer sclera.[51] These characteristics could be important in the local response to acute IOP, and, thus, in the progression of glaucomatous optic neuropathy, which is often regional.[36,53,54] Studies of the sensitivity of ONH biomechanics to various geometric and mechanical characteristics of the ocular tissues have shown that acute ONH biomechanics are much more sensitive to variations in the properties of the sclera adjacent to the ONH than more distant sclera.[3,6,8,12–14,17,29,55–58] Thus, for this study on the effects of IOP on the tissues of the ONH, we assumed a simplified scleral shell, and did not incorporate regional variations in thickness[59,60] and mechanical properties.[56,58,61–64]

Our intention in this work was to demonstrate the possibility of using dimensionality reduction techniques and the huge potential benefits of reducing the number of variables needed to describe the effects of IOP. We decided to do this, first, on studies of modest increases in IOP because these allow the use of linear material properties, which simplifies the interpretation of the results. Larger increases in IOP will require the use of nonlinear materials.[56,58,61–65] Still, we believe that there are very good reasons to study the effects on the ONH of modest increases in IOP.[9,15] First, normal IOP is much more common than elevated IOP, and, therefore, small variations in IOP are relevant to a larger group. Second, small IOP elevations may be particularly informative in understanding the pathogenesis of low-tension glaucoma. Third, as demonstrated here and elsewhere,[8,9,19,27] ONH biomechanics are complex, even with simplified geometries and material properties and small variations in IOP. We believe that a solid

understanding of ONH biomechanics at low pressures helps build an understanding at elevated IOPs.

The models incorporate only the acute effects of IOP, and, therefore, do not represent the long term remodeling processes that are likely to play a profound role in the development of glaucoma, which we and others are actively studying.[1,3,7,17,21,35,50,52–54,61,62,66–72] Also, by considering a homogeneous LC, the models presented here did not account for the effects of IOP on the laminar microstructure. The complex geometry and composition of the lamina pores and trabeculae have been hypothesized to contribute to determining the local mechanical effects of IOP.[2,3,17,21,36,72,73] Specifically, the cells attached to the matrix of the LC could be subjected to larger strains than those of the homogenized structure,[2,3,74] and the load-bearing collagen fibers in the peripheral trabeculae may carry larger longitudinal loads than those in the more central trabeculae.[17,21,56,69,72] For further discussion of the assumptions and limitations in the models and their implications, please consult one of our previous studies.[6,8,14]

In summary, we have shown that with a few carefully selected variables (the PC's), we were able to describe the response of an ONH to acute variations in IOP, which previously would have required 25 variables. Together the first four PCs accounted for 96% of the response variance. A small set of uncorrelated responses will make it much simpler to describe and understand the effects of IOP on the ONH, which will in turn help identify the range of sensitivities to elevated IOP, and the relationship between IOP and glaucomatous vision loss.

References

1. Quigley HA. Glaucoma: macrocosm to microcosm the Friedenwald lecture. *Invest Ophthalmol Vis Sci*. 2005;46: 2662–2670.
2. Sigal IA, Ethier CR. Biomechanics of the optic nerve head. *Exp Eye Res*. 2009;88:799–807.
3. Burgoyne CF, Downs JC, Bellezza AJ, Suh JK, Hart RT. The optic nerve head as a biomechanical structure: a new paradigm for understanding the role of IOP-related stress and strain in the pathophysiology of glaucomatous optic nerve head damage. *Prog Retin Eye Res*. 2005;24:39–73.
4. Strouthidis NG, Fortune B, Yang H, Sigal IA, Burgoyne CF. Longitudinal change detected by spectral domain optical coherence tomography in the optic nerve head and peripapillary retina in experimental glaucoma. *Invest Ophthalmol Vis Sci*. 2011;52:1206–1219.
5. Yang H, Downs JC, Sigal IA, Roberts MD, Thompson H, Burgoyne CF. Deformation of the normal monkey optic nerve head connective tissue after acute IOP elevation within 3-D histomorphometric reconstructions. *Invest Ophthalmol Vis Sci*. 2009;50:5785–5799.
6. Sigal IA, Flanagan JG, Ethier CR. Factors influencing optic nerve head biomechanics. *Invest Ophthalmol Vis Sci*. 2005; 46:4189–4199.
7. Yang H, Thompson H, Roberts MD, Sigal IA, Downs JC, Burgoyne CF. Deformation of the early glaucomatous monkey optic nerve head connective tissue after acute IOP elevation in 3-D histomorphometric reconstructions. *Invest Ophthalmol Vis Sci*. 2011;52:345–363.
8. Sigal IA. Interactions between geometry and mechanical properties on the optic nerve head. *Invest Ophthalmol Vis Sci*. 2009;50:2785–2795.
9. Sigal IA, Yang H, Roberts MD, Burgoyne CF, Downs JC. IOP-induced lamina cribrosa displacement and scleral canal expansion: an analysis of factor interactions using parameterized eye-specific models. *Invest Ophthalmol Vis Sci*. 2011;52: 1896–1907.
10. Sigal IA. An applet to estimate the IOP-induced stress and strain within the optic nerve head. *Invest Ophthalmol Vis Sci*. 2011;52:5497–5506.
11. Anderson MJ, Whitcomb PJ. *RSM Simplified: Optimizing Processes Using Response Surface Methods for Design of Experiments*. London: Productivity Press; 2005:292.
12. Sigal IA, Flanagan JG, Tertinegg I, Ethier CR. Finite element modeling of optic nerve head biomechanics. *Invest Ophthalmol Vis Sci*. 2004;45:4378–4387.
13. Sigal IA, Flanagan JG, Tertinegg I, Ethier CR. Modeling individual-specific human optic nerve head biomechanics. Part I: IOP-induced deformations and influence of geometry. *Biomech Model Mechanobiol*. 2009;8:85–98.
14. Sigal IA, Flanagan JG, Tertinegg I, Ethier CR. Modeling individual-specific human optic nerve head biomechanics. Part II: influence of material properties. *Biomech Model Mechanobiol*. 2009;8:99–109.
15. Sigal IA, Yang H, Roberts MD, et al. IOP-induced lamina cribrosa deformation and scleral canal expansion: independent or related? *Invest Ophthalmol Vis Sci*. 2011;52:9023–9032.
16. Sigal IA, Yang H, Roberts MD, Downs JC. Morphing methods to parameterize specimen-specific finite element model geometries. *J Biomech*. 2010;43:254–262.
17. Roberts MD, Sigal IA, Liang Y, Burgoyne CF, Downs JC. Changes in the biomechanical response of the optic nerve head in early experimental glaucoma. *Invest Ophthalmol Vis Sci*. 2010;51:5675–5684.
18. Heickell AG, Bellezza AJ, Thompson HW, Burgoyne CF. Optic disc surface compliance testing using confocal scanning laser tomography in the normal monkey eye. *J Glaucoma*. 2001;10: 369–382.
19. Sigal IA, Flanagan JG, Tertinegg I, Ethier CR. Predicted extension, compression and shearing of optic nerve head tissues. *Exp Eye Res*. 2007;85:312–322.
20. Sigal IA, Flanagan JG, Ethier CR. Factors influencing optic nerve head biomechanics. *Invest Ophthalmol Vis Sci*. 2005; 11:4189–4199.
21. Roberts MD, Liang Y, Sigal IA, et al. Correlation between local stress and strain and lamina cribrosa connective tissue volume fraction in normal monkey eyes. *Invest Ophthalmol Vis Sci*. 2010;51:295–307.
22. R_Development_Core_Team. *R: A Language and Environment for Statistical Computing*. Vienna, Austria: R Foundation for Statistical Computing; 2011:3441.
23. Montgomery DC. *Design and Analysis of Experiments*. 6th ed. Hoboken, NJ: Wiley; 2004:660.
24. Box GEP, Hunter JS, Hunter WG. *Statistics for Experimenters: Design, Innovation, and Discovery*. 2nd ed. Hoboken, NJ: Wiley-Interscience; 2005:664.
25. Moret F, Poloschek CM, Lagreze WA, Bach M. Visualization of fundus vessel pulsation using principal component analysis. *Invest Ophthalmol Vis Sci*. 2011;52:5457–5464.
26. Zuur AF, Ieno EN, Smith GM. *Analysing Ecological Data*. New York, NY: Springer; 2007:698.
27. Sigal IA, Bilonick RA, Kagemann L, et al. The optic nerve head as a robust biomechanical system. *Invest Ophthalmol Vis Sci*. 2012;53:2658–2667.
28. Sigal IA, Flanagan JG, Tertinegg I, Ethier CR. Reconstruction of human optic nerve heads for finite element modeling. *Technol Health Care*. 2005;13:313–329.
29. Girard MJ, Downs JC, Burgoyne CF, Suh JK. Peripapillary and posterior scleral mechanics—part I: development of an anisotropic hyperelastic constitutive model. *J Biomech Eng*. 2009;131:051011.

30. Girard MJ, Downs JC, Bottlang M, Burgoyne CF, Suh JK. Peripapillary and posterior scleral mechanics—part II: experimental and inverse finite element characterization. *J Biomech Eng*. 2009;131:051012.
31. Woo SL, Kobayashi AS, Schlegel WA, Lawrence C. Nonlinear material properties of intact cornea and sclera. *Exp Eye Res*. 1972;14:29–39.
32. Sander EA, Downs JC, Hart RT, Burgoyne CF, Nauman EA. A cellular solid model of the lamina cribrosa: mechanical dependence on morphology. *J Biomech Eng*. 2006;128:879–889.
33. Fatehee N, Yu PK, Morgan WH, Cringle SJ, Yu DY. The impact of acutely elevated intraocular pressure on the porcine optic nerve head. *Invest Ophthalmol Vis Sci*. 2011;52:6192–6198.
34. Strouthidis NG, Fortune B, Yang H, Sigal IA, Burgoyne CF. Effect of acute intraocular pressure elevation on the monkey optic nerve head as detected by spectral domain optical coherence tomography. *Invest Ophthalmol Vis Sci*. 2011;52:9431–9437.
35. Roberts MD, Grau V, Grimm J, et al. Remodeling of the connective tissue microarchitecture of the lamina cribrosa in early experimental glaucoma. *Invest Ophthalmol Vis Sci*. 2009;50:681–690.
36. Yan DB, Coloma FM, Metheetrairut A, Trope GE, Heathcote JG, Ethier CR. Deformation of the lamina cribrosa by elevated intraocular pressure. *Br J Ophthalmol*. 1994;78:643–648.
37. Agoumi Y, Sharpe GP, Hutchison DM, Nicolela MT, Artes PH, Chauhan BC. Laminar and prelaminar tissue displacement during intraocular pressure elevation in glaucoma patients and healthy controls. *Ophthalmology*. 2011;118:52–59.
38. Jonas JB, Budde WM, Nemeth J, Grundler AE, Mistlberger A, Hayler JK. Central retinal vessel trunk exit and location of glaucomatous parapapillary atrophy in glaucoma. *Ophthalmology*. 2001;108:1059–1064.
39. Girard MJ, Strouthidis NG, Ethier CR, Mari JM. Shadow removal and contrast enhancement in optical coherence tomography images of the human optic nerve head. *Invest Ophthalmol Vis Sci*. 2011;52:7738–7748.
40. Sigal IA, Flanagan JG, Tertinegg I, Ethier CR. 3D morphometry of the human optic nerve head. *Exp Eye Res*. 2010;90:70–80.
41. Lee EJ, Kim TW, Weinreb RN, Park KH, Kim SH, Kim DM. Visualization of the lamina cribrosa using enhanced depth imaging spectral-domain optical coherence tomography. *Am J Ophthalmol*. 2011;152:87–95.
42. Yamanari M, Lim Y, Makita S, Yasuno Y. Visualization of phase retardation of deep posterior eye by polarization-sensitive swept-source optical coherence tomography with 1-microm probe. *Opt Express*. 2009;17:12385–12396.
43. Vilupuru AS, Rangaswamy NV, Frishman LJ, Smith EL III, Harwerth RS, Roorda A. Adaptive optics scanning laser ophthalmoscopy for in vivo imaging of lamina cribrosa. *J Opt Soc Am A Opt Image Sci Vis*. 2007;24:1417–1425.
44. Ivers KM, Li C, Patel N, et al. Reproducibility of measuring lamina cribrosa pore geometry in human and nonhuman primates with in vivo adaptive optics imaging. *Invest Ophthalmol Vis Sci*. 2011;52:5473–5480.
45. Levy NS, Crapps EE. Displacement of optic nerve head in response to short-term intraocular pressure elevation in human eyes. *Arch Ophthalmol*. 1984;102:782–786.
46. Poostchi A, Wong T, Chan KC, et al. Optic disc diameter increases during acute elevations of intraocular pressure. *Invest Ophthalmol Vis Sci*. 2010;51:2313–2316.
47. Kakutani Y, Nakamura M, Nagai-Kusuhara A, Kanamori A, Negi A. Marked cup reversal presumably associated with scleral biomechanics in a case of adult glaucoma. *Arch Ophthalmol*. 2010;128:139–141.
48. Yoshikawa K, Inoue Y. Changes in optic disc parameters after intraocular pressure reduction in adult glaucoma patients. *Jpn J Ophthalmol*. 1999;43:225–231.
49. Hyvärinen A. Independent component analysis. *Survey on Independent Component Analysis*. 1999;2:94–128.
50. Fatehee N, Yu PK, Morgan WH, Cringle SJ, Yu DY. Correlating morphometric parameters of the porcine optic nerve head in spectral domain optical coherence tomography with histological sections. *Br J Ophthalmol*. 2011;95:585–589.
51. Winkler M, Jester B, Nien-Shy C, et al. High resolution three-dimensional reconstruction of the collagenous matrix of the human optic nerve head. *Brain Res Bull*. 2010;81:339–348.
52. Yan D, McPheeters S, Johnson G, Utzinger U, Vande Geest JP. Microstructural differences in the human posterior sclera as a function of age and race. *Invest Ophthalmol Vis Sci*. 2011;52:821–829.
53. Yang H, Downs JC, Girkin C, et al. 3-D Histomorphometry of the normal and early glaucomatous monkey optic nerve head: lamina cribrosa and peripapillary scleral position and thickness. *Invest Ophthalmol Vis Sci*. 2007;48:4597–4607.
54. Yang H, Williams G, Downs JC, et al. Posterior (outward) migration of the lamina cribrosa and early cupping in monkey experimental glaucoma. *Invest Ophthalmol Vis Sci*. 2011;52:7109–7121.
55. Grytz R, Meschke G. Constitutive modeling of crimped collagen fibrils in soft tissues. *J Mech Behav Biomed Mater*. 2009;2:522–533.
56. Grytz R, Meschke G. A computational remodeling approach to predict the physiological architecture of the collagen fibril network in corneo-scleral shells. *Biomech Model Mechanobiol*. 2010;9:225–235.
57. Norman RE, Flanagan JG, Sigal IA, Rausch SM, Tertinegg I, Ethier CR. Finite element modeling of the human sclera: influence on optic nerve head biomechanics and connections with glaucoma. *Exp Eye Res*. 2011;93:4–12.
58. Girard MJ, Dahlmann-Noor A, Rayapureddi S, et al. Quantitative mapping of scleral fiber orientation in normal rat eyes. *Invest Ophthalmol Vis Sci*. 2011;52:9684–9693.
59. Olsen TW, Aaberg SY, Geroski DH, Edelhauser HF. Human sclera: thickness and surface area. *Am J Ophthalmol*. 1998;125:237–241.
60. Norman RE, Flanagan JG, Rausch SM, et al. Dimensions of the human sclera: thickness measurement and regional changes with axial length. *Exp Eye Res*. 2010;90:277–284.
61. Coudrillier B, Tian J, Alexander S, Myers KM, Quigley HA, Nguyen TD. Mechanical response of the human posterior sclera: age- and glaucoma-related changes measured using inflation testing. *Invest Ophthalmol Vis Sci*. 2012;53:1714–1728.
62. Girard MJ, Suh JK, Bottlang M, Burgoyne CF, Downs JC. Biomechanical changes in the sclera of monkey eyes exposed to chronic IOP elevations. *Invest Ophthalmol Vis Sci*. 2011;52:5656–5669.
63. Elsheikh A, Geraghty B, Alhasso D, Knappett J, Campanelli M, Rama P. Regional variation in the biomechanical properties of the human sclera. *Exp Eye Res*. 2010;90:624–633.
64. Myers KM, Cone FE, Quigley HA, Gelman S, Pease ME, Nguyen TD. The in vitro inflation response of mouse sclera. *Exp Eye Res*. 2010;91:866–875.
65. Spoerl E, Boehm AG, Pillunat LE. The influence of various substances on the biomechanical behavior of lamina cribrosa and peripapillary sclera. *Invest Ophthalmol Vis Sci*. 2005;46:1286–1290.
66. Sigal IA, Yang H, Roberts MD, Burgoyne CF, Downs JC. Biomechanics of the posterior pole during remodeling progression from normal to early experimental glaucoma. Paper presented at: ASME 2009 Summer Bioengineering Conference; June 17–21, 2009; Lake Tahoe, CA.
67. Hernandez MR. The optic nerve head in glaucoma: role of astrocytes in tissue remodeling. *Prog Retin Eye Res*. 2000;19:297–321.

68. Crawford Downs J, Roberts MD, Sigal IA. Glaucomatous cupping of the lamina cribrosa: a review of the evidence for active progressive remodeling as a mechanism. *Exp Eye Res*. 2011;93:133–140.

69. Grytz R, Meschke G, Jonas JB. The collagen fibril architecture in the lamina cribrosa and peripapillary sclera predicted by a computational remodeling approach. *Biomech Model Mechanobiol*. 2011;10:371–382.

70. Albon J, Farrant S, Akhtar S, et al. Connective tissue structure of the tree shrew optic nerve and associated ageing changes. *Invest Ophthalmol Vis Sci*. 2007;48:2134–2144.

71. Jonas JB, Jonas SB, Jonas RA, Holbach L, Panda-Jonas S. Histology of the parapapillary region in high myopia. *Am J Ophthalmol*. 2011;152:1021–1029.

72. Grytz R, Sigal IA, Ruberti JW, Meschke G, Downs JC. Lamina cribrosa thickening in early glaucoma predicted by a microstructure motivated growth and remodeling approach. *Mech Mater*. 2012;44:99–109.

73. Brown DJ, Morishige N, Neekhra A, Minckler DS, Jester JV. Application of second harmonic imaging microscopy to assess structural changes in optic nerve head structure ex vivo. *J Biomed Opt*. 2007;12:024029.

74. Rogers RS, Dharsee M, Ackloo S, Sivak JM, Flanagan JG. Proteomics analyses of human optic nerve head astrocytes following biomechanical strain. *Mol Cell Proteomics*. 2012;11: M111.012302.